

# Block Spin Magnetic Phase Transition of $A_y\text{Fe}_{1.6}\text{Se}_2$ Under High Pressure

Chao Cao,<sup>1,\*</sup> Minghu Fang,<sup>2</sup> and Jianhui Dai<sup>1,2,†</sup>

<sup>1</sup>Condensed Matter Group, Department of Physics,  
Hangzhou Normal University, Hangzhou 310036, China

<sup>2</sup>Department of Physics, Zhejiang University, Hangzhou 310027, China  
(Dated: August 12, 2011)

We predict an unconventional magnetic ground state in  $A_y\text{Fe}_{1.6}\text{Se}_2$  with  $\sqrt{5} \times \sqrt{5}$  Fe-vacancy superstructure under hydraulic external pressure based on first-principles simulations. While the Fe-vacancy ordering persists up to at least  $\sim 12\text{GPa}$ , the magnetic ground state goes at  $\sim 10\text{GPa}$  from the BS-AFM phase to a Néel-FM phase, a ferromagnetic arrangement of a "Néel cluster". The new magnetic phase is metallic, and the BS-AFM to Néel-FM phase transition is accompanied by a sizable structural change. The two distinct magnetic phases can be understood within the extended  $J_1$ - $J_2$  Heisenberg model by assuming a pressure-tuned competition between the intrablock and interblock nearest-neighbor couplings of iron moments.

PACS numbers: 75.25.-j, 71.20.-b, 75.10.Hk

*Introduction.* The anti-PbO-type FeSe is the simplest Fe-based superconductor with  $T_c \sim 8\text{K}$ [1]. Recently, a class of new iron superconductors  $A_y\text{Fe}_{2-x}\text{Se}_2$  ( $A=\text{Tl,K,Rb,Cs}$ ) with enhanced  $T_c \sim 30\text{K}$ [2-4] has attracted intensive interest. These materials are structurally similar to the 122-type iron-pnictides[5] with the FeSe layers intercalated by the  $A$  atoms, leaving certain amount of Fe-vacancies in the Fe-square lattice. The iron-vacancies are expected to order in some periodic superstructures at certain  $x$  values[3]. Among the proposed superstructures, the  $\sqrt{5} \times \sqrt{5}$  vacancy ordering pattern(see in FIG. 1), corresponding to  $x = 0.4$ , seems to be of special importance since it exists in most of  $A_y\text{Fe}_{2-x}\text{Se}_2$  compounds as confirmed by experiments from neutron diffraction[6-9] to high-resolution transmission electron microscope[10].

In addition to the  $\sqrt{5} \times \sqrt{5}$  superstructure, a novel block-spin antiferromagnetism, the BS-AFM order shown in FIG.1(b) with large magnetic moment of irons, was discovered by the neutron diffraction experiments[6]. A remarkable observation is the co-existence of superconductivity and BS-AFM order in  $A_y\text{Fe}_{2-x}\text{Se}_2$ [6]. It has been debated whether the co-existence is intrinsic at the microscopic level[11], or due to phase separation[12]. Previous independent density functional theory (DFT) calculations show that the ground state has a BS-AFM order in the presence of the Fe-vacancy superstructure [13, 14]. Since the magnetic ordering temperature, which is unprecedentedly high ( $T_N \sim 550\text{K}$ ), is close to the Fe-vacancy ordering temperature  $T_V \sim 580\text{K}$ [6], it was also proposed that the Fe-vacancy ordering may be driven by magnetic exchange interactions so as to minimize the magnetic frustrations[15].

All these interesting issues are closely related to the Fe-vacancy orderings and call for further experimental investigations. A key to resolve these issues is to clarify whether the BS-AFM is the only magnetic ground state or whether there are other magnetic ground states in the

Fe-vacancy ordered compounds. Here we suggest to seek for these states by applying physical pressure, a clean parameter to tune the lattice and electronic structures. We note a recent high pressure experiment on superconducting sample of nominal  $\text{K}_{0.8}\text{Fe}_{1.7}\text{Se}_2$  compound, where the resistance hump is suppressed at a critical pressure of 8.7 GPa and  $T_c$  is suppressed at a similar pressure[16]. The metallic phase in the high pressure regime was believed to arise from charge transfer between two different Fe vacancy occupancies but its magnetic structure is unknown.

In this paper, we study the lattice and magnetic structures of  $A_y\text{Fe}_{1.6}\text{Se}_2$  under high pressure up to 16 GPa by using first-principles simulations. We find that while the BS-AFM ground state (which is insulating at  $y = 0.8$ [13, 14]) persists to 10GPa, a novel metallic magnetic phase, the Néel-FM phase, becomes the new ground state for higher pressures. Both the BS-AFM and Néel-FM phases can be described by the extended  $J_1$ - $J_2$  model while the magnetic phase transition is accompanied by a sizable structural change.

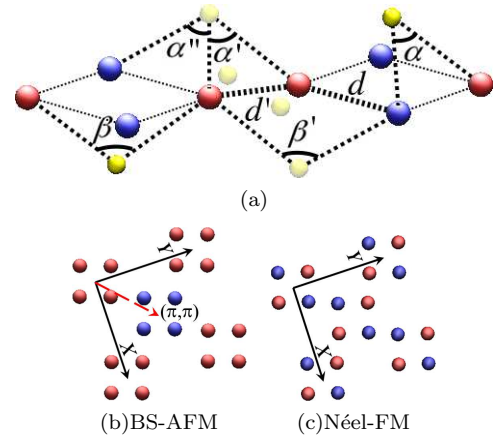


FIG. 1: The geometry (a) and magnetic patterns for (b) BS-AFM (AFM2) and (c) Néel-FM (AFM4). The structural parameters are as defined in FIG.2.

*Magnetic phases and ground state.* For the first principle simulations, plane-wave basis and projected augmented wave methods are used as implemented in VASP code [17, 18]. The Perdew, Burke, and Ernzerhoff flavour of generalized gradient approximation (GGA)[19] is employed to calculate the electron exchange-correlation energy. A 360 eV energy cutoff for the plane-waves and  $4 \times 4 \times 4$  Monkhorst-Pack k-grid[20] are chosen to ensure the total energy converges to 1 meV/Fe. The external pressure is introduced using the Pulay stress method. With the applied pressure, both the internal coordinates and the lattice constants are fully optimized for each calculated magnetic and non-magnetic configurations until the total force on each atom is  $< 0.01$  eV/Å. For the density of state (DOS) calculations, a dense  $16 \times 16 \times 16$   $\Gamma$ -centered k-grid, as well as the tetrahedra method are used to obtain accurate energy gap sizes. In the following text, we report and discuss detailed results for  $A=\text{Ti}$ , while the validity of all conclusions is checked for  $A=\text{K}$  and  $\text{Rb}$ .

We first identify the true ground state by examining the relative energies of several possible magnetic configurations[13, 21]. As shown in FIG. 2(a), the relative energetic order of different magnetic configurations vary drastically with the applied external pressure. The AFM2 pattern (the BS-AFM phase, FIG.1(b)) remains the ground state until around 10GPa, where the originally second highest AFM4 (FIG.1(c)) pattern takes over and eventually becomes the new ground state on the high pressure side. In the AFM4 phase, the four spins in each  $\text{Fe}_4$  block form a Néel order, while all block configurations are parallelly aligned, thus we denote it the Néel-FM phase for simplicity. The new ground state is at least 15 meV/Fe lower than all other calculated phases at 12 GPa, and is at least 20 meV/Fe lower at 16 GPa.

*Structure variation.* A close examination reveals the details of the vacancy-induced structural distortion during the process, as shown in FIG. 2(c)-(e). From 0 GPa to 10 GPa, the interblock nearest-neighbor (n.n.) Fe-Fe distance  $d'_{\text{Fe-Fe}}$  is compressed from 2.86Å to 2.64Å, more severely than the intrablock n.n. Fe-Fe distance  $d_{\text{Fe-Fe}}$  (from 2.62Å to 2.50Å). Meanwhile, all Fe-Se-Fe angles ( $\alpha$ ,  $\alpha'$ ,  $\alpha''$ ,  $\beta$ , and  $\beta'$ ) are slightly reduced. The formation of vacancy superstructures also causes the relative height of Fe atoms  $z_{\text{Fe}}$  (measured from the nearest Tl-layer) to be slightly different in two neighboring blocks. However, this distortion is negligible ( $z_{\text{Fe}}^1 - z_{\text{Fe}}^2 < 0.08\text{Å}$ ) in the BS-AFM state until 10 GPa.

The magnetic phase transition then occurs, together with a structural change, identified by the first abrupt volume change around 10GPa as shown in FIG.2(b). Across the transition,  $d_{\text{Fe-Fe}}$  expands to 2.61Å,  $d'_{\text{Fe-Fe}}$  is further reduced to 2.57Å, and  $\beta$  jumps from 94.35° to 104.61°. The lattice constant  $a$  expands from 8.17Å to 8.32Å, while  $c$  is severely compressed from 13.24Å to 12.41Å. The difference in  $z_{\text{Fe}}$  is enhanced from 0.07Å

to 0.26Å. After the transition, from 10 GPa to 14 GPa,  $d_{\text{Fe-Fe}}$  and  $d'_{\text{Fe-Fe}}$  also slightly drops, but all Fe-Se-Fe angles start to increase, and the difference in  $z_{\text{Fe}}$  keeps increasing as well.

Another abrupt change in Fe-Fe distances (and Fe-Se-Fe angles) could be identified from 14 GPa to 16 GPa (FIG.2(b)), as the lattice constant  $a$  abnormally expands from 8.27Å to 8.40Å and  $c$  collapses from 11.95Å to 11.03Å. A closer examination reveals that the difference in  $z_{\text{Fe}}$  expands abruptly from 0.32Å at 14 GPa to 0.73Å at 16 GPa. This severe change implies that the backbone of vacancy superstructure is becoming unstable and that the superstructure may break down under such high pressure. Thus we focus on the magnetic phase transition around 10 GPa in the following discussions.

*Extended  $J_1$ - $J_2$  Heisenberg model.* In order to understand the physics behind the pressure-induced magnetic phase transition we fit the energetics of the magnetic configurations using the extended  $J_1$ - $J_2$  model [13](FIG. 3(a)) where  $J_1$  and  $J_2$  (or  $J'_1$  and  $J'_2$ ) are the intrablock (or the interblock) n.n. and next-nearest-neighbor (n.n.n.) exchange couplings, respectively.  $J'_2$  is always AFM, for pressure from 0 GPa to 16 GPa; while  $J_1$ ,  $J'_1$  and  $J_2$ , being FM at 0 GPa, become AFM at approximately 8 GPa, 6 GPa, and 11 GPa, respectively. All  $J$ s increase monotonically with increasing pressure, except for  $J_2$  which dwells around -20 meV until 10GPa. We notice that for ambient pressure the fitted values of  $J$ s are compatible with the low energy spin wave excitations probed in the recent experiment[22], while in the high pressure Néel-FM phase, the fitted values are compatible with the Monte Carlo result[23].

Variations of these exchange interactions, while reflecting complicated electronic structures that evolve with pressure, can be attributed to a combined effect of the electron correlation ( $U$ ), the Hund's coupling ( $J_H$ ), the crystal field splitting, as well as various short-ranged hopping integrals at the microscopic five-orbital Hubbard model level. As inferred from the previous DFT study for the iron pnictides[24],  $J_H$  plays an important role in mapping out the local magnetic interactions though  $U$  involved in GGA calculations may be not large. Some insights can be gained if we adopt the intuitive results obtained from perturbation or Hartree-Fock mean-field theory[25, 26]. The n.n. and n.n.n. exchange couplings are then contributed from two virtual processes where Fe-3d electrons hop between two sites directly, or via p-orbitals of the Se-atoms[24]. The contribution from the direct exchange depends strongly on the inter-atomic distances, while the contribution from the indirect exchange depends strongly on both the inter-atomic distance and the Fe-Se-Fe angle.

On one hand, both contributions decrease monotonically with Hund's coupling and become FM at relatively large  $J_H/U$ . On the other hand, for fixed  $J_H/U$ , the second contribution could be ferromagnetic when the an-

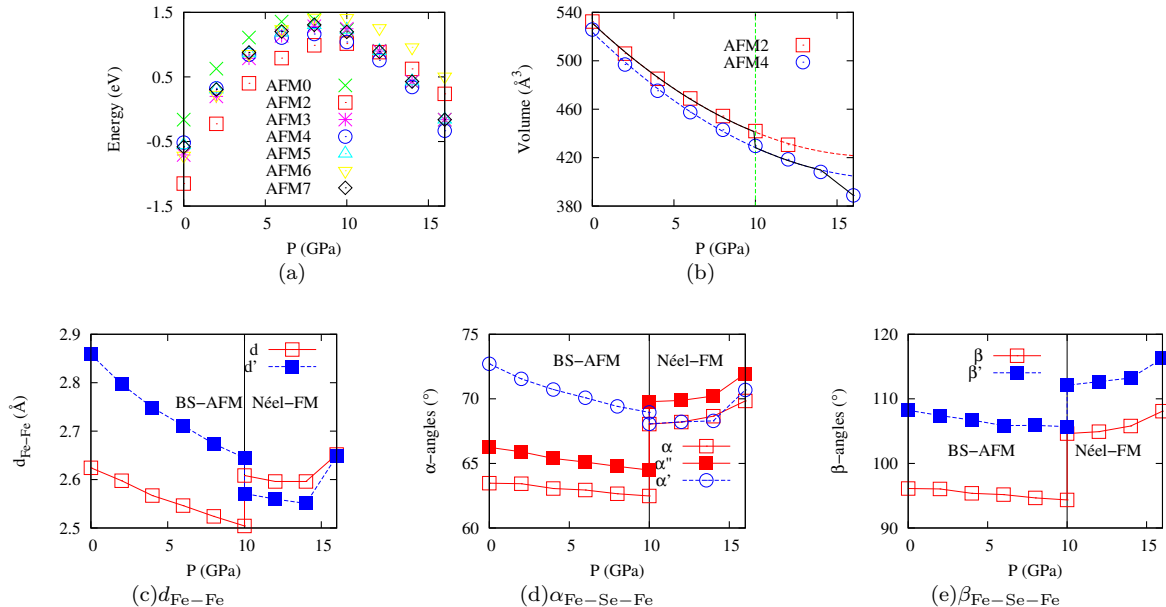


FIG. 2: Variation of magnetic configuration energies and structural parameters with respect to external pressure. (a) Total energy per unit cell of different magnetic phases. To enhance the visibility, the total energies have been renormalized using  $\tilde{E}(P) = E(P) - kP + E_0$  with  $k = 2.800$  eV/GPa and  $E_0 = 120.163$  eV. (b) Unit cell volume of BS-AFM and Néel-FM phases, where the black solid line indicates the actual volume per unit cell. (c)-(e) Various structural parameters as defined in Fig. 1(a)

gle  $\gamma = (\pi - \beta)/2$  formed by the Fe-Se bond and the Fe plane is larger than a certain threshold value varying in between  $35^\circ \sim 40^\circ$  approximately, depending on the details of materials[26]. From our structural analysis, the threshold values of  $\gamma$  calculated by the structure parameters for the corresponding fitted  $J_1$ ,  $J'_1$ , and  $J_2$  are about  $36^\circ \sim 42^\circ$ , which reasonably fall into the FM region given by the mean-field approximation[26]. Meanwhile, the  $\gamma$  angle associated with  $J'_2$  is the smallest (about  $35^\circ$  or less) due to the structural distortion. It explains why  $J_1$ ,  $J'_1$ , and  $J_2$  are initially FM and increase under pressure, while  $J'_2$  is AFM even for ambient pressure. It is interesting to remark that across the phase transition,  $\beta$  angle abruptly changes from  $94.35^\circ$  to  $104.61^\circ$ , leading to a sign change in the second contribution, and thus  $J_2$  becomes AFM around 10 GPa. From 10 GPa to 14 GPa, not only Fe-Fe distances are reduced, but the Fe-Se-Fe angles (or  $\gamma$ ) are also increased (reduced), thus all  $J$ s rapidly increases.

Once the two competing phases, namely the BS-AFM and Néel-FM phases, are identified as shown in FIG.2(a), the magnetic phase transition point should be at  $J_1 = J'_1/2$ , when the energy of the Néel-FM phase is equal to that of the BS-AFM phase. Using this criterion and the least-square-fitting of the  $J$ s, we determine the critical pressure to be 10.53GPa. Hence the phase transition around 10 GPa is mainly driven by competition between  $J_1$  and  $J'_1$ , while the role of  $J_2$  or  $J'_2$  is to stabilize the BS-AFM phase or the Néel-FM phases in the respective

low or high pressure regimes[27].

*Band structure and density of states.* The transition from the BS-AFM to Néel-FM phases drastically changes the electronic structure of the material. It was shown that  $A_{0.8}Fe_{1.6}Se_2$  is an AFM insulator with the band gap  $\sim 400$ -600 meV [13, 14]. Here, the gap size  $E_g$  and the magnetic moment per Fe atom  $m_{Fe}$  of  $Tl_{0.8}Fe_{1.6}Se_2$  in the BS-AFM or the Néel-FM states are calculated and shown in FIG. 3(b).

In the BS-AFM phase, when the pressure increases from 0 to 10GPa, the intra- and inter-block Fe-Fe n.n. distances greatly reduce, which enhance the hopping between the n.n. Fe atoms, resulting in a decrease of  $E_g$  from  $\sim 400$  meV to  $\sim 100$  meV. Meanwhile,  $m_{Fe}$  starts from  $2.81 \mu_B$  at 0GPa and gradually reduces to  $2.40 \mu_B$  at 10GPa. The rapid suppression of  $E_g$  compared with the small variation of  $m_{Fe}$  reveals possible vacancy-enhanced Mott physics [28–30].

By contrary, we find that the Néel-FM phase is always metallic as shown in FIG.3(b). We have also checked that the metallicity is robust until  $U \sim 4$  eV by using GGA+ $U$  calculations. Therefore, for  $y = 0.8$ , the magnetic phase transition is associated with an insulator-metal phase transition. In the Néel-FM phase,  $m_{Fe}$  sets off from  $2.52 \mu_B$  at 0GPa, and is reduced to  $1.66 \mu_B$  at 10 GPa. It reaches the lowest value of  $1.27 \mu_B$  at 14GPa, where the collapsed phase transition occurs and restores  $m_{Fe}$  to  $1.40 \mu_B$  at 16GPa. It is important to notice that although the Néel block ensures vanishing net moment

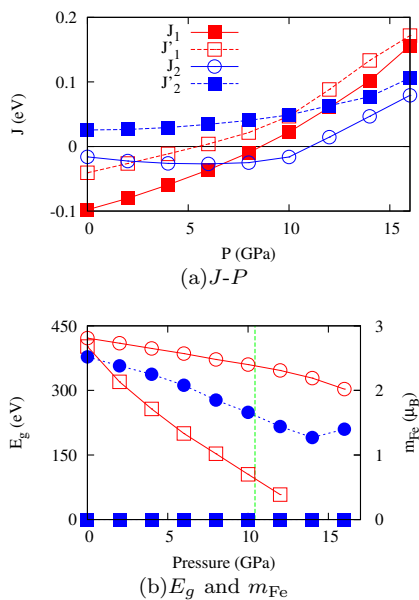


FIG. 3: The variation of electronic structure with respect to external pressure. (a) Exchange-coupling constants fitted using the extended  $J_1$ - $J_2$  model, and (b) band gap size  $E_g$  and magnetic moment per Fe  $m_{Fe}$ . In panel (b), the open/filled circles and squares denote  $m_{Fe}$  and  $E_g$  at the BS-AFM/Néel-FM phases, respectively.

in the classic ordering configuration, there is no overall  $\mathbf{q}$ -vector ensuring the time-reversal symmetry, since the blocks are ferromagnetically aligned.

*Discussions.* The magnetic states considered in this paper are based on the classical Heisenberg model, and the  $m_{Fe}$ , which is about  $2.5\mu_B$ - $3.0\mu_B$  in the BS-AFM phase, should be considered as the static local magnetic moment. This is in agreement with the neutron diffraction experiment where a large iron moment  $3.31\mu_B/Fe$  (for  $A=K$ ) was reported [6]. Therefore quantum fluctuations should be suppressed in the ordered phases due to the large magnetic moment. One expects that quantum fluctuations play a larger role when the magnetic transition point is approached, but the two magnetic phases should be robust in the presence of the vacancy superstructure. The magnetic phase transition is likely of first order because it is accompanied with a sizable change in the lattice constants. An adequate account of quantum fluctuations needed for a thorough understanding of the transition calls for future studies.

Our results shed a new light in understanding the available high pressure experiment[16] if the resistance hump observed in most of the superconducting samples of  $A_yFe_{2-x}Se_2$  is interpreted as due to a phase separation involving a Fe-vacancy disordered superconducting phase and a Fe-vacancy ordered BS-AFM insulating phase, respectively. With this interpretation, the metallic phase in the high pressure regime is not necessarily due to the charge transfer between two iron sites of different occu-

pancies as previously expected, but due to the Néel-FM phase which respects the  $\sqrt{5} \times \sqrt{5}$  vacancy ordering. Of course, the accompanied structural distortion, in particular the difference in  $z_{Fe}$ , may complicate the comparison with experiments.

We would like to thank Elihu Abrahams and Qimiao Si for careful reading of the manuscript as well as for useful discussions. This work has been supported by the NSFC, the NSF of Zhejiang Province (No.Z6110033), the 973 Project of the MOST. All calculations were performed at the High Performance Computing Center of Hangzhou Normal University College of Science.

\* E-mail address: ccao@hznu.edu.cn

† E-mail address: daijh@zju.edu.cn

- [1] F. Hsu et al, Proc. Natl. Acad. Sci. **105**, 14262 (2008).
- [2] J. Guo et al, Phys. Rev. B **82**, 180520(R) (2010).
- [3] M. Fang et al, Europhys. Lett. **94**, 27009 (2011).
- [4] H. Wang et al, Europhys. Lett. **93**, 47004 (2011).
- [5] M. Rotter, M. Tegel, and D. Johrendt, Phys. Rev. Lett. **101**, 107006 (2008).
- [6] W. Bao et al, Chin. Phys. Lett. **28**, 086104 (2011).
- [7] F. Ye et al., arXiv:1102.2882 (2011).
- [8] J. Bacsa et al., Chem. Sci. **2**:1054 (2011).
- [9] V.Y. Pomjakushin et al., J. Phys.: Condensed Matter **23**, 156003 (2011).
- [10] Z. Wang et al., Phys. Rev. B **83**, 140505 (2011).
- [11] R.H. Liu et al., Europhys. Lett. **94**, 27008 (2011).
- [12] F. Chen et al., arXiv:1106.3026 (2011).
- [13] C. Cao and J. Dai, Phys. Rev. Lett. **107**, 056401 (2011).
- [14] X.M. Yan et al., Phys. Rev. B **83**, 233205 (2011).
- [15] C. Fang et al., arXiv:1103.4599 (2011).
- [16] J. Guo et al., arXiv:1101.0092 (2011).
- [17] G. Kresse and J. Hafner, Phys. Rev. B **47**, 558 (1993).
- [18] G. Kresse and D. Joubert, Phys. Rev. B **59**, 1758 (1999).
- [19] J. Perdew, K. Burke, and M. Ernzerhof, Phys. Rev. Lett. **77**, 3865 (1996).
- [20] H.J. Monkhorst and J.D. Pack, Phys. Rev. B **13**, 5188 (1976).
- [21] For the details of the considered magnetic configurations and the stability of vacancy superstructures, please refer to supplementary information(SI).
- [22] M. Wang et al., arXiv:1105.4675 (2011).
- [23] R. Yu, P. Goswami, and Q. Si, arXiv:1104.1445 (2011).
- [24] F. Ma, Z.-Y. Lu, and T. Xiang, Phys. Rev. B **78**, 224517 (2008).
- [25] Q. Si and E. Abrahams, Phys. Rev. Lett. **101**, 076401 (2008).
- [26] M. Caldeon et al., arXiv:1107.2279 (2011).
- [27] When the structural distortion is sufficiently small under certain circumstances, another magnetic phase, the AFM7 phase (see SI) formed by ferromagnetically coupled collinear-AFM spin blocks, could compete with the Néel-FM phase and become the ground state.
- [28] C. Cao and J. Dai, Phys. Rev. B **83**, 193104 (2011).
- [29] R. Yu, J.X. Zhu, Q. Si, Phys. Rev. Lett. **106**, 186401 (2011).
- [30] Y. Zhou et al., Europhys. Lett. **95**, 17003 (2011).

## SUPPLEMENTARY INFORMATION

## Definition of magnetic patterns

We consider several possible ground states with magnetic configurations or patterns as illustrated in FIG.(S-1), and we list their total energy under specific pressure in TAB.(S-I). These states can be captured by the extended  $J_1$ - $J_2$  Heisenberg model in the classical limit

$$H = \sum_{\langle i,j \rangle \text{intra}} J_1 S_i S_j + \sum_{\langle i,j \rangle \text{inter}} J'_1 S_i S_j + \sum_{\langle\langle i,j \rangle\rangle \text{intra}} J_2 S_i S_j + \sum_{\langle\langle i,j \rangle\rangle \text{inter}} J'_2 S_i S_j.$$

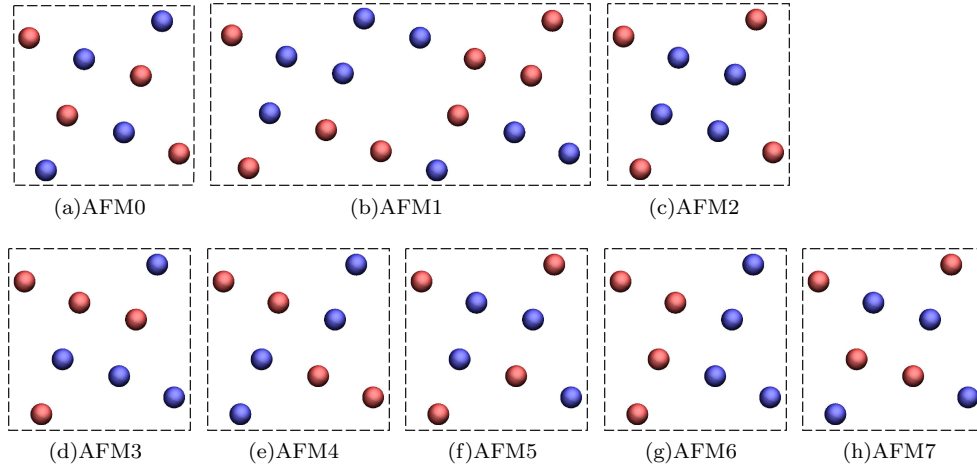


FIG. S-1: The magnetic structures considered.

TABLE S-I: Total energies (in eV) per unit cell of different magnetic configurations at different pressures.

P(GPa)	AFM0	AFM1	AFM2	AFM4	AFM5	AFM6	AFM7
0	-120.163	-121.152	-120.709	-120.517	-120.559	-120.719	-120.583
2	-113.772	-114.625	-114.201	-114.076	-114.094	-114.175	-114.094
4	-107.688	-108.397	-108.010	-107.956	-107.932	-107.942	-107.919
6	-101.841	-102.405	-102.061	-102.088	-102.013	-101.956	-101.994
8	-96.207	-96.607	-96.313	-96.431	-96.295	-96.178	-96.289
10	-90.767	-90.980	-90.750	-90.955	-90.766	-90.581	-90.798
12	-85.489	-85.510	-85.494	-85.635	-85.496	-85.138	-85.505
14	-80.366	-80.169	-80.364	-80.450	-80.364	-79.834	-80.366
16	-75.355	-74.955	-75.355	-75.526	-75.355	-74.685	-75.355

### Energy expressions

The eigen energies of each states per block are listed as follows:

$$E_{\text{AFM0}} = (-4J_1 - 2J'_1 + 2J_2 + 4J'_2)S^2 \quad (\text{S1})$$

$$E_{\text{AFM1}} = 0 \quad (\text{S2})$$

$$E_{\text{AFM2}} = (4J_1 - 2J'_1 + 2J_2 - 4J'_2)S^2 \quad (\text{S3})$$

$$E_{\text{AFM3}} = -2J_2S^2 \quad (\text{S4})$$

$$E_{\text{AFM4}} = (-4J_1 + 2J'_1 + 2J_2 - 4J'_2)S^2 \quad (\text{S5})$$

$$E_{\text{AFM5}} = -2J'_1S^2 \quad (\text{S6})$$

$$E_{\text{AFM6}} = (2J'_1 - 2J_2)S^2 \quad (\text{S7})$$

$$E_{\text{AFM7}} = (-2J'_1 - 2J_2)S^2 \quad (\text{S8})$$

### Bi-collinear phase cannot be ground state

In our discussions, the conventional FM phase as well as the bi-collinear AFM phase (AFM1, Fig. S-1(b)) observed in some 11-type iron chalcogenides are excluded from the ground state candidates.

Firstly, we have performed simulations at 12 GPa, confirming that the bi-collinear and FM phases are about  $\sim 13$  meV/Fe and  $\sim 19$  meV/Fe higher than the Néel-FM phase, respectively.

Secondly, based on the extended  $J_1$ - $J_2$  model, it is straightforward to show that the bi-collinear phase could not be the ground state when the  $\sqrt{5} \times \sqrt{5}$  vacancy superstructure is preserved.

*Proof:* If the bi-collinear phase (AFM1) were the ground state, we could obtain from Eqn. S1 and Eqn. S3:  $-4J_1 - 2J'_1 + 2J_2 + 4J'_2 > 0$  and  $4J_1 - 2J'_1 + 2J_2 - 4J'_2 > 0$ , respectively. Adding them together yields  $-J'_1 + J_2 > 0$ . However, this condition contradicts Eqn. S7, which yields  $J'_1 - J_2 > 0$ . Therefore, the bi-collinear phase could not be the ground state of the extended  $J_1$ - $J_2$  model for any  $J$ s. The extra next-nearest-neighbor exchanges  $J_3$  and  $J'_3$  are needed for this state to be the ground state as in the conventional  $J_1$ - $J_2$ - $J_3$  model.

### Stability of vacancy superstructure at high pressure

We have performed simulations using  $5 \times 5$  supercell (230 atoms in all) with 3 randomly distributed Fe-vacancy patterns to verify that the vacancy superstructure remains robust under high pressure at least up to 12GPa. At 12GPa, the disordered vacancy superstructures are at least 4 meV/Fe higher than non-magnetic  $\sqrt{5} \times \sqrt{5}$  phase, and are at least 23 meV/Fe higher than the Néel-FM phase.

### Critical point for the BS-AFM/Néel-FM phase transition

For large positive  $J'_2$  or negative  $J_2$ , the ground state could be either the BS-AFM state or the Néel-FM state. The competition is given by  $E_{\text{BS-AFM}} - E_{\text{Néel-FM}} = E_{\text{AFM2}} - E_{\text{AFM4}} = 4S^2(2J_1 - J'_1)$ . Hence the critical point is  $J_1 = J'_1/2$ .

### Band structure and DOS of the Néel-FM phase

In the Néel-FM phase, the band structure indicates an electron pocket for majority spin and a hole pocket for minority spin around  $\Gamma$ . Two large electron pockets can also be identified for the majority spin around  $X$ , where no structure exists for the minority spin. If the occupancy of Tl sites is reduced by 20% ( $\text{Tl}_{0.8}\text{Fe}_{1.6}\text{Se}_2$ ), the electron pocket around  $\Gamma$  disappears due to the hole doping, and two hole pockets form around  $\Gamma$ . In this case, one another hole pocket also shows up around  $X$ . The electron states around  $E_F$  are dominated by the Fe-3d orbitals, while the Fe-3d and Se-4p orbitals hybridize over a wide range from  $E_F-8$  eV to  $E_F+2$  eV.

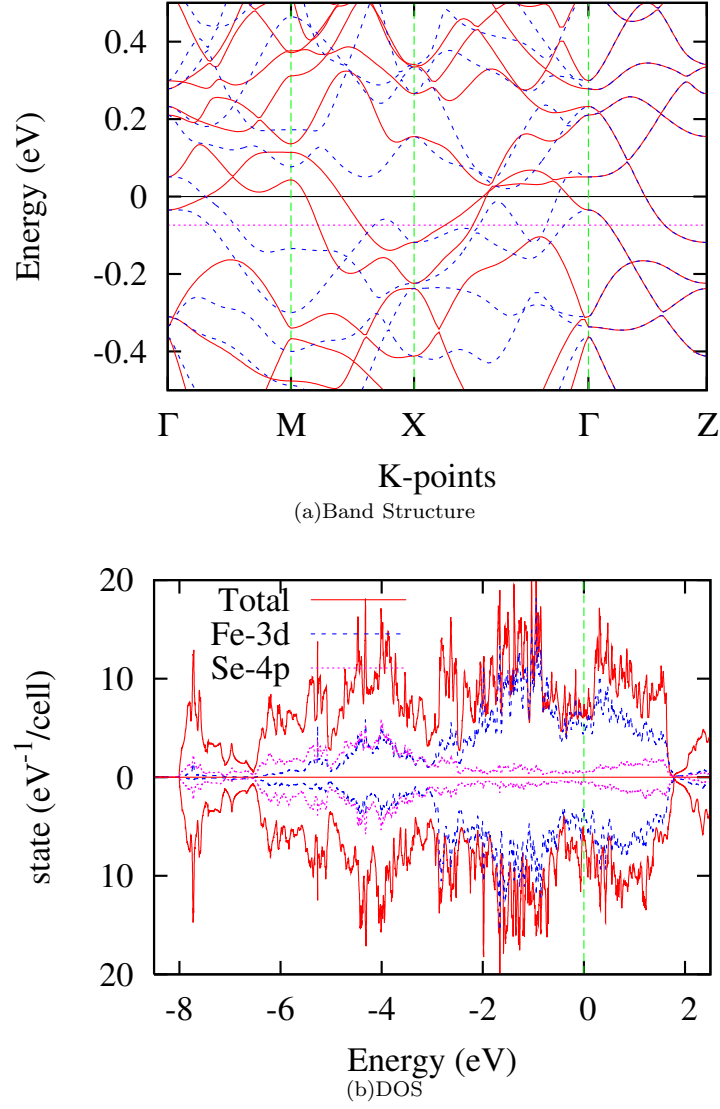


FIG. S-2: a) Band structure and b) DOS of Néel-FM  $\text{TlFe}_{1.6}\text{Se}_2$  at 12GPa. Notice that majority (solid red line in band structure; upper panel in DOS) and minority (dashed blue line in band structure; lower panel in DOS) spins are not degenerate in the  $k_x$ - $k_y$  plane, but are degenerate along  $k_z$ .